Synthesis of Single-Crystalline Co_3O_4 Octahedral Cages with Tunable Surface Aperture and Their Lithium Storage Properties

Xi Wang,[†,‡] Lingjie Yu,[§,‡] Xing-Long Wu,[†,‡] Fangli Yuan,[§] Yu-Guo Guo,[†] Ying Ma,*[,†] and Jiannian Yao*[,†]

Beijing National Laboratory for Molecular Science, Key Laboratory of Photochemistry, Institute of Chemistry, Chinese Academy of Sciences, Beijing 100190, People's Republic of China, Institute of Process Engineering, Chinese Academy of Sciences, Beijing 100190, People's Republic of China, and Graduate University of the Chinese Academy of Sciences, Beijing 100049, People's Republic of China

Received: May 18, 2009; Revised Manuscript Received: July 1, 2009

In this paper, single-crystalline Co_3O_4 hollow octahedral hollow cages with tunable surface aperture were synthesized by the carbon-assisted carbothermal method. On the basis of electron microscopic observation and structural analysis, all the following factors, including the precursor concentration, species of precursor, intrinsic crystal structure of products and carbon-assisted carbothermal reaction, play key roles in the formation of Co_3O_4 octahedral hollow structures. When the as-prepared Co_3O_4 samples were used as the anode materials in lithium ion batteries (LIBs), it was found that the octahedral hollow cages with large surface aperture performed better than both those with small surface aperture and Co_3O_4 nanoparticles, indicating that not only the single-crystalline robust structure but also the tunable surface aperture in the shell could affect the electrochemical property in LIBs.

1. Introduction

Transition metal oxides with hollow structures have received considerable interests as a class of materials because of their wide applications in various fields.[1−13] Among them, Co_3O_4 hollow structure has been paid special attention due to its potential applications in catalysts, adsorbents, sensors, and lithium ion batteries.[9−13] As a new class of anode materials for lithium ion batteries (LIBs) discovered in 2000,[18] Co_3O_4 can deliver three times larger than the theoretical capacity of currently used graphite (<372 mAh g^{-1}). However, one of the major challenges for the practical use of Co_3O_4-based materials is capacity fading over multiple charge−discharge cycles caused by the large volume changes that accompany Li insertion−deinsertion. To resolve this problem, many hollow structured Co_3O_4 electrode materials have been synthesized nowadays,[13,15,16] because the large void space could enhance their capacity retention by reversibly accommodating large volume expansion. Most researches focused on the Co_3O_4 hollow spherical structure,[10,16] while the well-defined nonspherical hollow structures rarely have been reported.[15]

Since Li et al. reported the synthesis of the colloidal carbon spheres (CCSs),[18] CCSs have been paid considerable attention as hard templates to prepare hollow structures due to the simple control and uniform products.[19−21] In previous work, we have fabricated single-crystalline octahedral NiO nanocages by using CCSs as templates.[3] In this work, we successfully synthesized Co_3O_4 hollow octahedral cages with tunable surface aperture via the carbon-assisted carbothermal method. When tested for the anode material in LIBs, the single-crystalline Co_3O_4 hollow octahedra demonstrated much higher Li^+ storage capacities and better cycling performance than Co_3O_4 nanoparticles; the improved electrochemical performance could be attributed to their unique architecture. The superior electrochemical performance and easy synthesis of these Co_3O_4 hollow octahedral cages may suggest their practical use in LIBs.

2. Experimental Section

2.1. Chemicals and Reagents. All chemicals (analytical grade) were purchased from Beijing Chemicals Corp., China, and used as received without further purification.

2.2. Synthesis of Octahedral Co_3O_4 Hollow Crystals. In a typical experiment, $CoCl_2 \cdot 6H_2O$ was added in 10 mL distilled water to form 0.005−0.5 M solution. Then 0.2−0.5 g of as-prepared carbon spheres, which were synthesized according to the literature,[18] were dispersed in the above $CoCl_2$ solution. After ultrasonic treatment for 40 min, the resulting suspension was aged for 24 h and then oven-dried at 60 °C. Finally, the oven-dried powders were heated at 450−600 °C in a furnace in air for 1−3.5 h and kept in the furnace until cooling to room temperature.

2.3. Characterization. The sizes and morphologies of the as-obtained samples were characterized by a field emission scanning electron microscope (FESEM, JSM-6700F, JEOL, Japan), a transmission electron microscope (TEM, H-700, Hitachi, Japan), and a high-resolution transmission electron microscope (HRTEM, JSM-2010, JEOL, Japan) operating at 200 kV. Phases were identified in an X-ray diffractometer (XRD, X-Pert, PANalytic, Netherlands) with Cu Kα radiation (40 kV, 30 mA). Electrochemical experiments were performed using 2032-coin cells. The working electrodes prepared by mixing the Co_3O_4 samples, acetylene black, and poly(vinyl difluoride) (PVDF) at a weight ratio of 70:20:10, were pasted on pure Cu foil (99.6%, Goodfellow). Glass fiber (GF/D) from Whatman was used as a separator. Lithium foil was used as the counter electrode. The electrolyte consisted of a solution of 1 M $LiPF_6$ in ethylene carbonate (EC)/dimethyl carbonate (DMC)/diethyl

* To whom correspondence should be addressed. Phone: +86-10-82616517. Fax: +86-10-82616517. E-mail: (J.Y.) jnyao@iccas.ac.cn; (Y.M.) yingma@iccas.ac.cn.
[†] Institute of Chemistry, Chinese Academy of Sciences.
[‡] Graduate University of the Chinese Academy of Sciences.
[§] Institute of Process Engineering, Chinese Academy of Sciences.

10.1021/jp904652m CCC: $40.75
Published on Web 08/12/2009

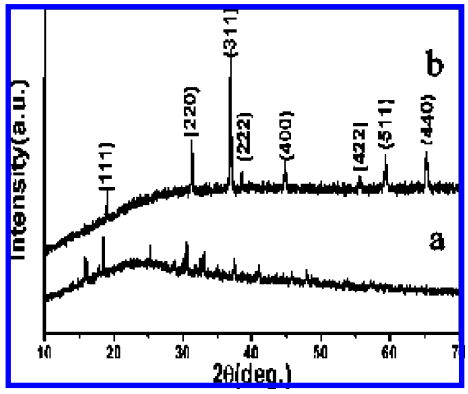

Figure 1. XRD patterns of as-synthesized products after drying treatment at 60 °C and calcination at 480 °C: (a) $CoCl_2 \cdot 6H_2O$, (b) Co_3O_4.

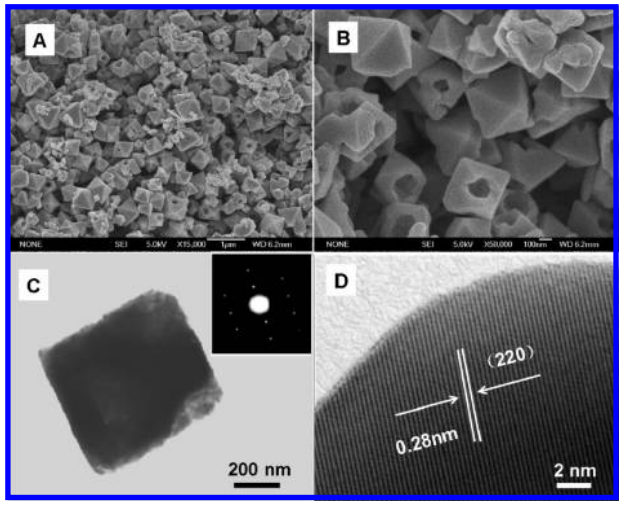

Figure 2. (A) SEM image of Co_3O_4 hollow octahedral crystals obtained after calcining precursors (0.02 M of $CoCl_2$, 0.4 g CCSs), (B) the large-scale SEM image, (C) the TEM image of a single Co_3O_4 hollow octahedron and SEAD pattern (inset), and (D) the corresponding HRTEM image.

carbonate (DEC) (1:1:1, in wt %) obtained from Ferro Corp. A galvanostatic cycling test of the assembled cells was carried out on an LAND CT2001A system in the voltage range of 0.01−3.0 V (vs Li^+/Li) at a discharge/charge rate of C/5 (178 mA g^{-1}).

3. Results and Discussion

3.1. Structure. The crystal structures of products were confirmed by X-ray diffraction (XRD). Figure 1a shows the XRD pattern of products after drying treatment at 60 °C, and the recorded diffraction peaks are well-assigned to the structure of $CoCl_2 \cdot 6H_2O$. It indicates that no hydroxylation took place for $CoCl_2$ in solution. When calcined at 480 °C, the diffraction peaks typical of face-centered cubic (fcc) Co_3O_4 are clearly observed (line b), which agree with those of standard Co_3O_4 of cubic structure (JCPDS Card No. 42-1467).[13] No impurities such as precursor compounds have been detected, indicating the formation of pure cobalt oxides.

3.2. Morphologies. Figure 2A shows a typical SEM image of Co_3O_4 products obtained after calcination. All the samples show octahedral shape. It is noticed that the yield of the octahedral structures is as high as 90% in our work. The edge length of the octahedral cages is ~600 nm. Figure 2B shows a high-magnification FESEM image of the cracked Co_3O_4 octahedra with a broken hole on their surface, which confirms that the Co_3O_4 octahedra are indeed hollow. It is also worth noting that the holes on cracked octahedra generally lie at or near their apexes, which might be associated to their weak stress points at the octahedral apexes and arris. From the TEM image (Figure 2C), one can see that the center of the individual particle is brighter than the edge, further illuminating their hollow nature. The SAED pattern corresponding to individual hollow octahedron is inserted in Figure 2C, which shows the hollow octahedron is single-crystalline structure as indicated by the clear diffraction spots. A HRTEM image of the edge area of such a hollow octahedron is shown in Figure 2D. The lattice fringe of d_{220} was measured at about 2.8 Å, which was in good agreement with the face-centered cubic Co_3O_4 (JCPDS Card No. 42-1467).

Similar to the formation of NiO octahedral cages,[3] cobalt precursors underwent both the phase and shape changes during calcination as shown in Supporting Information, Figure S1 and S2. As the calcination time increased, the precursors gradually transformed from $CoCl_2$, to the mixture of $CoCl_2$ and Co_3O_4, and finally to pure Co_3O_4. Correspondingly, the morphology changed from spherical, to spherelike and octahedron-like, to octahedral, and the surface of the products gradually evolved from rough to smooth. It is believed that recrystallization took place during carbothermal reaction[3] (between Co_3O_4 and carbon) as discussed below.

3.3. Effect of Precursor. ***3.3.1. Influence of Precursor Concentration on the Surface Aperture and Shell-Thickness of Co_3O_4 Hollow Octahedra.*** It is demonstrated that the surface aperture of Co_3O_4 products can be actively controlled by adjusting the reaction precursor concentration. When the concentration of $CoCl_2$ is at a low level (0.006 M), the octahedron-like Co_3O_4 hollow products each with a large hole on the surface are observed (Figure 3A). The holes are so large that nearly all particles are cracked. Increasing precursor concentration up to 0.01 M, the Co_3O_4 particles basically are the octahedral ones but the holes on their surfaces become small (Figure 3B). Elevating the concentration to 0.03 M causes the smaller aperture on the octahedral surface (Figure 3C), compared with those obtained at 0.006 and 0.01 M.

It is also noticed that the precursor concentration plays an important role in shell-thickness of the octahedral Co_3O_4 hollow structures as shown in Figure 3. In fact, the shell-thickness of these hollow structures gradually increased as the concentration was elevated. From the SEM image shown in Figure 3A, one can see that the obtained products clearly exhibit hollow structure and the shell thickness can be easily identified as ~80 nm. Compared with Figure 3A, Figure 3B clearly reveals an increase of shell thickness (into 150 nm) and a decrease in interior cavity size. The formation of samples with different shell thicknesses and open apertures may be attributed to the $CoCl_2$ shells with different thicknesses formed at drying stage.

3.3.2. Influence of Precursor Species on the Morphology of the Final Products. In the typical synthesis, chlorine ions play an important role in the formation of octahedral shape. For comparison, we did the similar experiments with other cobalt salts (such as $Co(CH_3COO)_2$ and $Co(NO_3)_2$) as precursors under the same conditions; unfortunately, only small nanoparticles with irregular morphology shown in Figure 4A,B were observed. Furthermore, only polycrystalline Co_3O_4 hollow spheres (Figure 4C,D) can be obtained when cleaning Cl^- ions for several times using water before calcination of the mixture. Energy dispersive X-ray (EDX) analysis on water rinsed mixture clearly showed the existence of elemental Co and an atomic ratio of Co to Cl greater than 3:1 (Supporting Information, Figure S3). This result

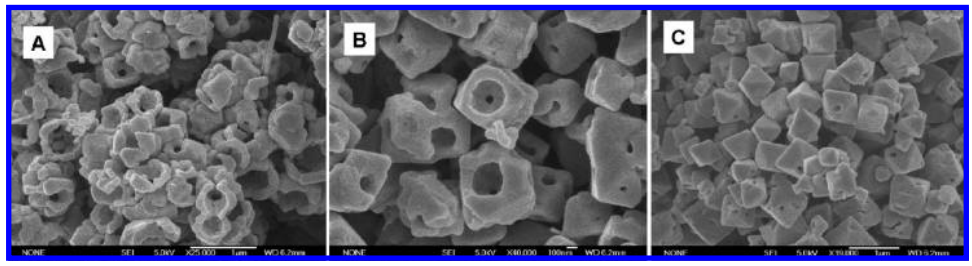

Figure 3. Low-magnification FESEM images of the Co_3O_4 hollow octahedra obtained at different concentrations with the addition of 0.4 g CCSs: (A) 0.006, (B) 0.01, and (C) 0.03 M.

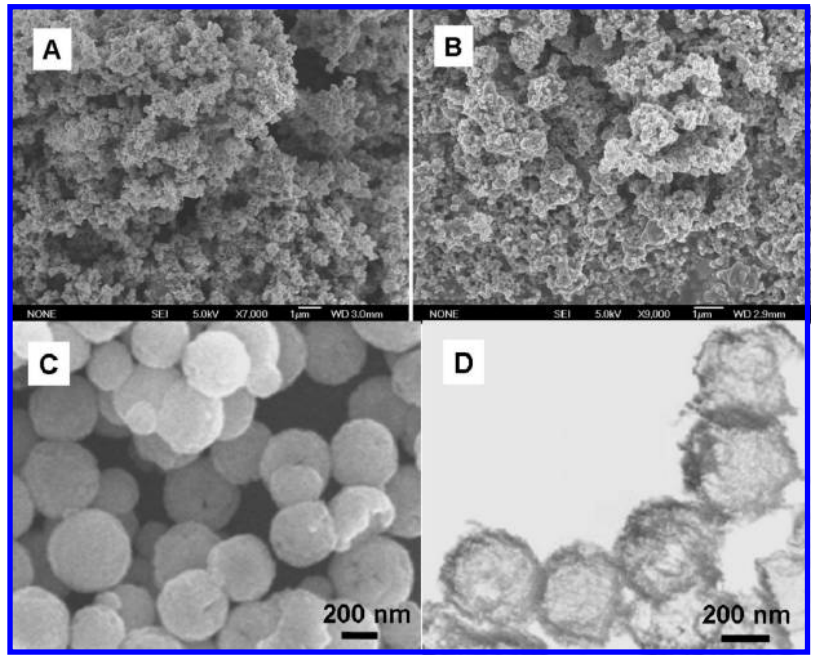

Figure 4. SEM images of the products using the different precursors: (A) $Co(Ac)_2$, (B) $Co(NO_3)_2$; (C,D) SEM and TEM images of Co_3O_4 hollow spheres obtained after calcining water rinsed precursors.

indicates that Co^{2+} ions were selectively absorbed in the surface layer and Cl^- ions were partly cleaned since the ratio of Co^{2+} to Cl^- in bulk solution was 1:2. The polysaccharide-like layer at the surface of carbon spheres may serve as an adsorbent, which can chelate Co^{2+} ions.[18] On the basis of the above analysis, it is clear that the octahedral structures can be formed when the precursors were chlorides.

It is well known that the shape of the final products in solid-state reactions depends on the rate of nucleation and growth. Chlorine ions can usually be used as a functional group and adsorbed at the surface of particles, restricting the advance of grain boundaries during annealing,[22] simultaneously, the diffusion of solid particles at ambient temperature is often of short-range, thus helping to yield micro- and nanosized products. For example, Sun et al. reported that the single-crystalline SnO_2 nanorods have been successfully synthesized by using chloride salt-assisted additive to control the size of precursors in the solid-state reaction and to inhibit crystal growth during annealing.[22] Baranov also synthesized single-crystal ZnO nanorods with assistance of NaCl.[23] In our case, it is believed that the cagelike shells of chlorine salt surrounding CCSs play key role in the formation of single-crystalline structures. The chloride salt is helpful for not only controlling the size of precursors in the solid-state reaction but also inhibiting crystallite growth in the oriented aggregation process.

3.4. Effect of Intrinsic Crystal Structure. Besides chlorine salt-assisted role for the formation of octahedral morphologies, the intrinsic crystal habits of materials also play important role on the final shape. In the present work, we also chose $MnCl_2$, $CuCl_2$, and $FeCl_3$ as starting materials respectively, the morphologies of the corresponding products after calcination are shown in Figure 5. From these images, one can see that only manganic oxide particles are likely octahedral and the other products are basically irregular polyhedral but not octahedral. It may be attributed to their different intrinsic crystal structures, because manganic oxide products obtained have body-centered cubic structure and copper oxide and iron oxide belong to monoclinic system. So far only Co_3O_4 and NiO_3 octahedral hollow structures can be acquired in our lab. The octahedral shape may therefore be intrinsically attributed to its face-centered cubic crystal structure for which the formation of {111} surface planes is favorable.[24] In addition, Ran et al.[25] reported that solid octahedral Co_3O_4 structures could be synthesized by reaction of $CoCl_2$ in molten $NaNO_3$, because the mass mobility could be quickened in the molten salt, which helped Co_3O_4 follow octahedral growth of itself crystal habit.[26]

3.5. Influence of Solvents on the Morphology of the Final Products. Except for water system (solution), we also chose ethanol as the solvent to do above study. It is found that the perfect octahedral Co_3O_4 hollow structures can also be synthesized. Figure 6A shows the low-scale SEM image of Co_3O_4 products, suggesting the regular octahedral shape. Figure 6B shows a high-magnification FESEM image of an individual

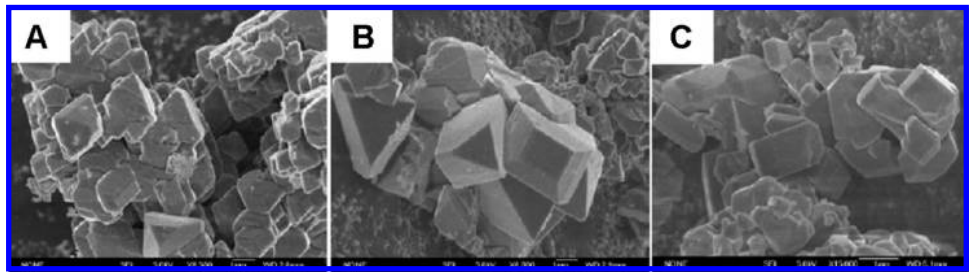

Figure 5. SEM images of the products using other metal chlorides with the addition of 0.4 g CCSs: (A) $MnCl_2$, (B) $CuCl_2$, (C) $FeCl_3$.

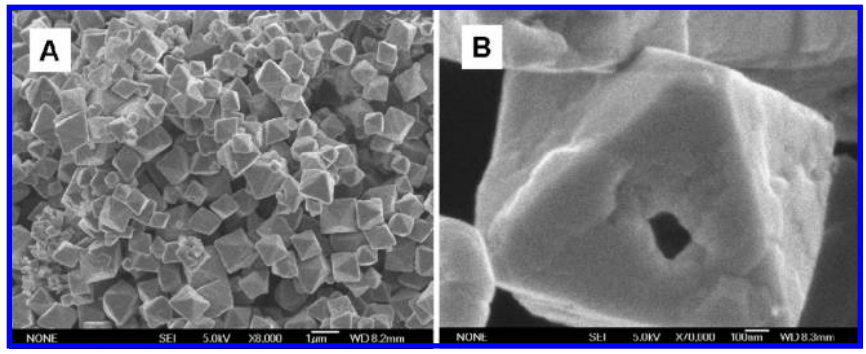

Figure 6. SEM images of the Co_3O_4 products using $CoCl_2$ ethanolic solution with the addition of 0.4 g CCSs.

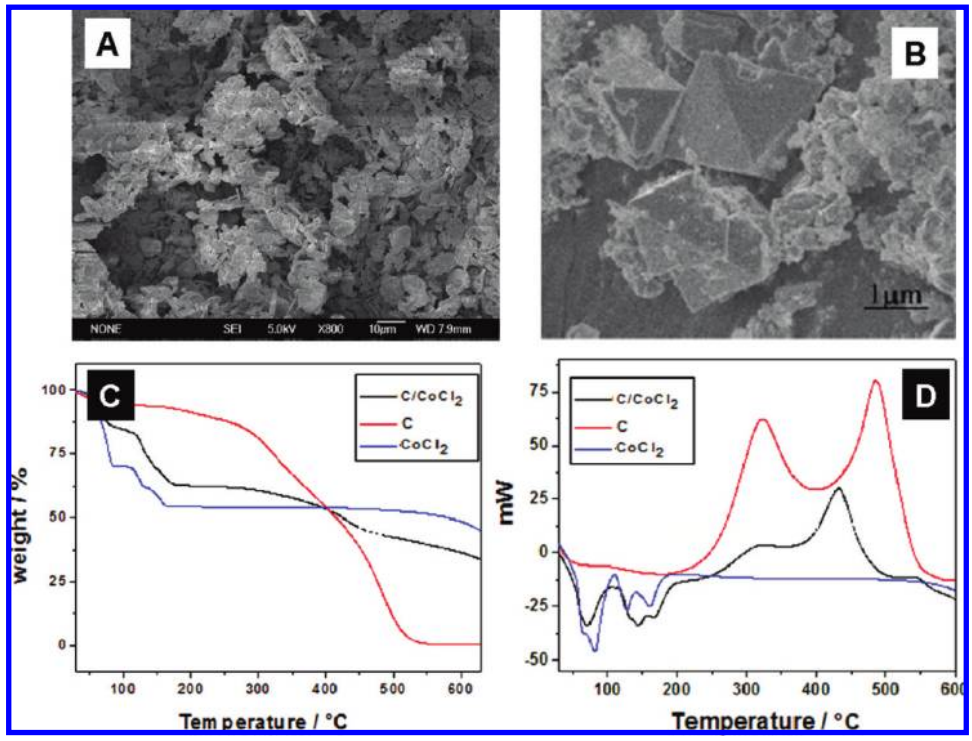

Figure 7. SEM images of the products after calcination: (A) $CoCl_2$, (B) 1:10 $CoCl_2$ and CCSs mixture; (C,D) TGA and DSC spectra of samples.

Co_3O_4 particle with a broken hole, which confirms that the octahedra are indeed hollow.

3.6. Important Role of Template-Assisted Carbothermal Reaction. In order to investigate the role of carbon templates on the formation of octahedral hollow structure, $CoCl_2$ as starting material without adding carbon templates was calcined. As an example, 2 g of pure $CoCl_2 \cdot 6H_2O$ was heated at 500 °C for 1.5 h and some crystalline Co_3O_4 were detected in products by XRD; however, the octahedral particles have not been found in products by SEM. As shown in Figure 7A, the morphology of products was of irregular crystal aggregates. When we took the mixture of $CoCl_2$ and CCSs with the weight ratio of 1:10 as the precursor, Co_3O_4 octahedral products could also be obtained after calcination (Figure 7B). Comparing the two experimental results, it is concluded that carbothermal reaction (between Co_3O_4 and carbon) may be helpful for the formation of single-crystalline Co_3O_4 octahedral products. It is reasonable that carbon can offer a weak reductive environment to promote nuclei oriented growth in the solid state reaction.[27−32]

TGA results of samples are shown in Figure 7C. For pure $CoCl_2 \cdot 6H_2O$, there are two major zones of mass loss mainly in range from room temperature to 161.45 °C attributed to

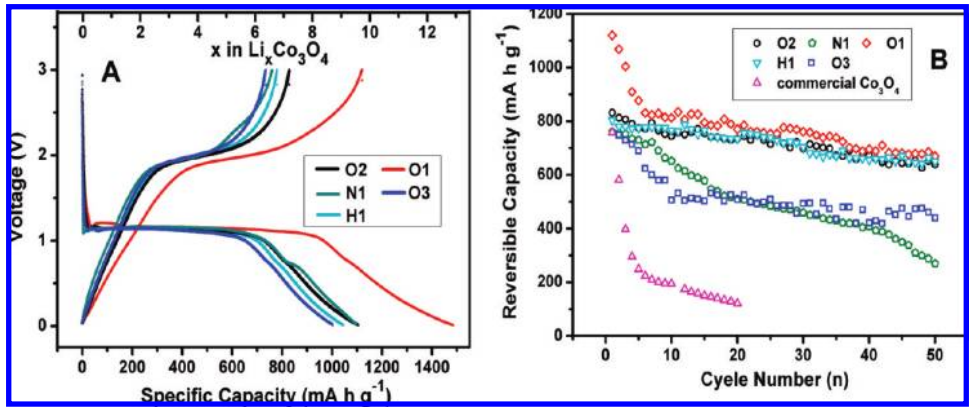

Figure 8. (A) Voltage profiles of the Co_3O_4 samples with different morphologies between 0 and 3 V at a rate of 178 mA/g for the first cycle, and (B) reversible capacities vs the cycle number.

dehydration and oxidation of $CoCl_2 \cdot 6H_2O$, respectively, and the corresponding mass loss is about 29.92 and 15.77%. It is worth noting that there is basically no mass loss in range from 161.45 to 550 °C, indicating nearly all $CoCl_2 \cdot 6H_2O$ transforming into Co_3O_4. This can also be testified by DSC analysis shown in Figure 7D in which there is no exothermic or endothermic peak between 161.45 and 550 °C. For the sample CCSs, there are two major zones of mass loss with a total mass loss of ~93.63%. A slow weight loss peaking at 320.27 °C (DSC spectrum, Figure 7D) is attributed to the further dehydration and densification of carbon spheres, and the sharp weight loss peaking at 484 °C is attributed to burning of the carbon spheres.

From both TGA and DSC spectra of the sample C/$CoCl_2 \cdot xH_2O$, one can find some interesting phenomena compared to CCSs and the pure $CoCl_2 \cdot xH_2O$. First, both the TGA and DSC profiles for C/$CoCl_2 \cdot xH_2O$ and $CoCl_2 \cdot xH_2O$ are similar before 200 °C. The similarity (Figure 7C,D) reveals that the two samples experience similar oxidation procedures. That is, nearly all $CoCl_2 \cdot xH_2O$ can transform into Co_3O_4 before 200 °C, thus CCSs-core/Co_3O_4-shell structures can be formed before this temperature. Second, there are both similarity and difference after 200 °C between the spectrum shapes of C/$CoCl_2 \cdot xH_2O$ and CCSs. The similarity is a slow loss of weight peaking at ~320 °C in DSC spectrum, attributed to the further dehydration and densification of carbon spheres. The first major difference is the temperature at which CCSs are burned. For the sample C/$CoCl_2 \cdot xH_2O$, the weight-loss peak attributed to the burning of CCSs shifts to a higher temperature of ~530 °C, compared to 484.44 °C for pure CCSs. This indicates that Co_3O_4 shell early formed on the surface of CCSs might inhibit the inner oxidation. In the meantime, there is a narrow and sharp exothermic peak at 433.73 °C for sample C/$CoCl_2 \cdot xH_2O$, which is not found in the curves of both CCSs and pure $CoCl_2 \cdot xH_2O$. The transformation of CCSs into CO gas followed by the recrystallization of Co_3O_4 crystals (Co_3O_4 shell) into octahedral structures may be responsible for this process.[4,27,28,30] From the above discussion, we can conclude that the carbon not only acts as a template, but also promotes the formation of Co_3O_4 octahedra. The experimental results also support this hypothesis. When the mixed precursors were calcined at lower temperatures at which no carbon combustion happens, only spherical products were obtained (Supporting Information, Figure S4-5).

On the basis of above analysis, it is believed that the formation of perfect single-crystal, octahedral hollow structures by using this method must meet the following requirements: (1) being chlorides for precursor; (2) being fcc structures for the corresponding oxides; and (3) carbon-assisted carbothermal reaction.

3.7. Lithium-Ion Battery Properties. In the recent 10 years, Co_3O_4 has attracted much attention as an anode electrode material for LIBs because of its superior theoretical capacity as well as lower cost and toxicity. To study the potential of the Co_3O_4 hollow octahedra as an electrode material in LIBs and the effect of morphology on the capacity of the electrode, the as-prepared Co_3O_4 samples with different morphologies, hollow quasi-octahedra (Figure 3A, 0.006 M precursor, hereinafter designated as O1), hollow octahedra (Figure 2, 0.02 M precursor, O2), hollow octahedra (Figure 3C, 0.03 M precursor, O3), hollow spheres (Figure 4C,D, H1), and nanoparticles (Figure 4A, N1), were measured by using the standard Co_3O_4/Li half-cell configuration at a constant current density of 178 mA/g (C/5).

Figure 8A shows first cycle discharge−charge voltage profiles for all five samples. The profiles are similar and consistent with previous reports,[33−37] indicating the same electrochemical pathway. For all samples, the two voltage plateaus between 1.3 and 1.1 V can be found from the first discharge curve, which are generally attributed to the reduction processes to $Li_xCo_3O_4$ and metallic Co, respectively.[12] As revealed in Figure 8A, the first discharge capacity of the sample O1, O2, H1, O3, and N1 is about 1470.2, 1100.1, 1044.2, 1003.2, and 1096.7 mA h g^{-1}, respectively, all of which are larger than the theoretical capacity (890 mA h g^{-1}). This is usually ascribed to irreversible reactions (e.g., decomposition of electrolyte) to form a solid electrolyte interphase (SEI) layer.[33−37] From the fully discharged state, the corresponding Coulombic efficiency is 76.2 (O1), 75.6 (O2), 74.7 (H1), 74.6 (O3), and 69.2% (N1), respectively. It is well known that a large irreversible loss at the first cycle is inevitable for most electrode materials. Apparently, O1 has the highest initial capacities and the lowest irreversible loss in all samples. It is speculated to result from their large open cavities of hollow octahedra to enhance Li storage and single-crystalline structures to increase stability. In the present case, the initial charge capacity of the four samples decreases in the following order: O1 > O2 > N1 > O3. This may be associated to the Brunauer−Emmett−Teller (BET) specific surface area, because the sample O1 has a relatively higher BET value of 18.1 m^2 g^{-1}, and O2, N1, and O3 have relatively lower values (10.3, 8.0, and 4.8 m^2 g^{-1}). The sample H1 exhibits similar initial charge capacity to N1, while its BET value is unknown due to the small amount.

Figure 8B shows the cycle number vs the charge capacities of the Co_3O_4 samples with different morphologies up to 50 cycles. The capacities of O1, H1, O2, O3, and N1 after 50 cycles are 670, 654, 639, 433, and 270 mAh/g, respectively. For comparison, commercial Co_3O_4 was also tested and its capacity

faded greatly after 20 cycles. Apparently, hollow samples have the better cycling performance than solid nanoparticles and commercial Co_3O_4. The improved lithium storage capacity of O1 might be attributed to their hollow structures[13] and the single-crystalline robust structures.[12] Hollow structures can buffer against the volume change during lithium insertion−deinsertion, hence alleviating the problem of pulverization of the electrode material and improving the cycling performance. Also, the single-crystalline robust structures guarantee good stability and improved crystallinity compared to those amorphous or polycrystalline ones.[12] Among the three hollow-structured single crystalline samples, O1 and O2 with larger surface aperture and a thinner shell have the best cycling performance, because the large surface aperture may provide extra space for the storage of lithium ions and the thin shells may be help for reducing effective diffusion distance for lithium ions. This is also the case for hollow spherical Co_3O_4 samples (H1). On the basis of all the above results, as-prepared hollow octahedral Co_3O_4 with appropriate surface aperture have excellent lithium storage properties and may become a new anode material for the next-generation LIBs.

4. Conclusions

In conclusion, novel Co_3O_4 hollow octahedral cages were synthesized by the carbon-assisted carbothermal method. Surface aperture of these cages can be modulated through adjusting the reaction conditions. The formation mechanism has been studied through systematic analysis of various experimental parameters, including the precursor concentration, species of precursor, intrinsic crystal structure of products and CCSs-assisted carbothermal reaction. It is believed that the formation of perfect single-crystal, octahedral hollow structures by this method must follow the following conditions: (1) being chlorides for precursor; (2) being fcc structures for the final oxides; and (3) carbon-assisted carbothermal reaction. When tested for electrochemical lithium storage, the as-prepared Co_3O_4 octahedral cages with large open surface aperture and single-crystalline robust structures exhibit very low initial irreversible loss, high reversible capacity, and excellent capacity retention over 50 cycles. We believe such a unique nanostructure (robust, octahedral cage) may also find other uses in novel applications such as sensors and catalysts.

Acknowledgment. This work was supported by National Natural Science Foundation of China (Nos. 20733006, 20871117, 50730005), the CAS/SAFEA International Partnership Program for Creative Research Teams, and the National Basic Research Program of China (2006CB806200).

Supporting Information Available: This material is available free of charge via the Internet at http://pubs.acs.org.

References and Notes

(1) Caruso, F.; Shi, X. Y.; Caruso, R. A.; Susha, A. *Adv. Mater.* **2001**, *13*, 740.
(2) Wang, X.; Hu, P.; Yuan, F.; Yu, L. *J. Phys. Chem. C* **2007**, *111*, 6706.
(3) Wang, X.; Yu, L.; Hu, P.; Yuan, F. *Cryst. Growth Des.* **2007**, *7*, 2415.
(4) Lou, X. W.; Archer, L. A.; Yang, Z. *Adv. Mater.* **2008**, *20*, 3987.
(5) Cao, A. M.; Hu, J. S.; Liang, H. P.; Wan, L. J. *Angew. Chem., Int. Ed.* **2005**, *44*, 4391.
(6) Chen, J.; Xu, L.; Li, W.; Gou, X. *Adv. Mater.* **2005**, *17*, 582.
(7) Guo, Y.-G.; Hu, J.-S.; Wan, L.-J. *Adv. Mater.* **2008**, *20*, 2878.
(8) Zhang, W.-M.; Hu, J.-S.; Guo, Y.-G.; Zheng, S.-F.; Zhong, L.-S.; Song, W.-G.; Wan, L.-J. *Adv. Mater.* **2008**, *20*, 1160.
(9) Cao, A.-M.; Hu, J.-S.; Liang, H.-P.; Song, W.-G.; Wan, L.-J.; He, X.-L.; Gao, X.-G.; Xia, S.-H. *J. Phys. Chem. B* **2007**, *111*, 15858.
(10) Zhao, W.; Liu, Y.; Li, H.; Zhang, X. *Mater. Lett.* **2008**, *62*, 772.
(11) He, T.; Chen, D.; Jiao, X.; Wang, Y. *Adv. Mater.* **2006**, *18*, 1078.
(12) Lou, X. W.; Deng, D.; Lee, J. Y.; Archer, L. A. *J. Mater. Chem.* **2008**, *18*, 4397.
(13) Lou, X. W.; Deng, D.; Lee, J. Y.; Feng, J.; Archer, L. A. *Adv. Mater.* **2008**, *20*, 258.
(14) Poizot, P.; Laruelle, S.; Grugeon, S.; Dupont, L.; Tarascon, J. M. *Nature* **2000**, *407*, 496.
(15) Li, W. Y.; Xu, L. N.; Chen, J. *Adv. Funct. Mater* **2005**, *15*, 851.
(16) Tao, F.; Gao, C.; Wen, Z.; Wang, Q.; Li, J.; Xu, Z. *J. Solid State Chem.* **2009**, *182*, 1055.
(17) Du, N.; Zhang, H.; Chen, B.; Wu, J.; Ma, X.; Liu, Z.; Zhang, Y.; Yang, D.; Huang, X.; Tu, J. *Adv. Mater.* **2007**, *19*, 4505.
(18) Sun, X.; Li, Y. *Angew. Chem., Int. Ed.* **2004**, *43*, 3827.
(19) Lou, X. W.; Yuan, C.; Archer, L. A. *Small* **2007**, *3*, 261.
(20) Nam, K. T.; Kim, D. W.; Yoo, P. J.; Chiang, C. Y.; Meethong, N. P.; Hammond, T.; Chiang, Y. M.; Belcher, A. M. *Science* **2006**, *312*, 885.
(21) Lou, X. W.; Wang, Y.; Yuan, C.; Lee, J. Y.; Archer, L. A. *Adv. Mater.* **2006**, *18*, 2325.
(22) Sun, J. Q.; Wang, J. S.; Wu, X. C. *Cryst. Growth. Des.* **2006**, *6*, 1584.
(23) Baranov, A. N.; Panin, G. N.; Kang, T. W. *Nanotechnology* **2005**, *16*, 1918.
(24) Yang, H. G.; Zeng, H. C. *Angew. Chem., Int. Ed.* **2004**, *43*, 5930.
(25) Ran, S.; Gao, L. *Chem. Lett.* **2007**, *36*, 688.
(26) Lim, Y. S.; Park, J. W.; Hong, S. T. *Mater. Sci. Eng. B* **2006**, *129*, 100.
(27) Gundiah, G.; Govindaraj, A.; Rao, C. N. R. *Chem. Phys. Lett.* **2002**, *351*, 189.
(28) Lao, J. Y.; Wen, J. G.; Ren, Z. F. *Nano Lett.* **2002**, *2*, 1287.
(29) Zhu, Y.; Bando, Y.; Xue, D.; Golberg, D. *J. Am. Chem. Soc.* **2003**, *125*, 16196.
(30) Jie, J.; Wang, G.; Han, X.; Fang, J.; Xu, B.; Yu, Q.; Liao, Y.; Li, F.; Hou, J. *J. Cryst. Growth* **2004**, *267*, 223.
(31) Wang, F.; Jin, G.; Guo, X. *J. Phys. Chem. B* **2006**, *110*, 14546.
(32) Zhao, H.; Lei, M.; Yang, X.; Jian, J.; Chen, X. *J. Am. Chem. Soc.* **2005**, *127*, 15722.
(33) Binotto, G.; Larcher, D.; Prakash, A. S.; Urbina, R. H.; Hegde, M. S.; Tarascon, J. M. *Chem. Mater.* **2007**, *19*, 3032.
(34) Laruelle, S.; Grugeon, S.; Poizot, P.; Dolle, M.; Dupont, L.; Tarascon, J. M. *J. Electrochem. Soc.* **2002**, *149*, A627.
(35) Kang, Y. M.; Song, M. S.; Kim, J. H.; Kim, H. S.; Park, M. S.; Lee, J. Y.; Liu, H. K.; Dou, S. X. *Electrochim. Acta* **2005**, *50*, 3667.
(36) Shaju, K. M.; Jiao, F.; Debart, A.; Bruce, P. G. *Phys. Chem. Chem. Phys.* **2007**, *9*, 1837.
(37) Li, Y. G.; Tan, B.; Wu, Y. Y. *Nano Lett.* **2008**, *8*, 265.

JP904652M